

## Chapter 5

### Effect of Non-Rectangular Spectra on Receiver Sensitivity

Receiver performance analysis performed thus far in this work has mainly assumed ideal rectangular spectra for all of the filters in the fiber link. The goal of this chapter is to discuss the effect of non-rectangular and more practical filter shapes on the receiver sensitivity of OOK and FSK spectrum-sliced systems. Optical bandpass filters used in the transmitter and receiver are now taken to have practically realizable impulse responses, and receiver sensitivity is calculated in terms of the 3 dB bandwidths of the optical filters.

The analysis is organized as follows: In Section 5.1 we discuss various optical filters used in contemporary fiber communication systems, and the modeling of the transfer functions of these filters. The mathematical formulation of the problem is discussed in Section 5.2, followed by the analysis of the receiver sensitivity for OOK transmission, as a function of not only  $m = B_oT$ , but also  $N$ , the order of the band-pass filter. In this chapter we will assume that these filters are based on the Fabry-Perot interferometer, and can be modeled under certain conditions to be Butterworth in passband. This analysis is performed in Section 5.3 for OOK using both the Gaussian approximation and an approximation that assumes the energy at the receiver decision circuit to be chi-square distributed. The case of FSK transmission and the corresponding results are obtained in Section 5.4, followed by a comparison of OOK and FSK in Section 5.5, and a summary of the chapter and the major results in Section 5.6.

It should be noted that only the case of an optical preamplifier receiver is treated since we have already shown in earlier chapters that it possesses a number of advantages over PIN receivers. **More importantly, unlike the case of rectangular spectra treated earlier, the “channel” seen by the signal and noise is now different** The signal path now contains two optical filters,

one used to spectrum-slice at the transmitter, and the other used to reject ASE noise in the preamplifier and also to select the appropriate WDM channel. Since the chief source of noise is the optical preamplifier, the noise path contains only one filter. Also note that we assume the receiver electrical filter to be of the integrate-and-dump type throughout our analysis. This is a reasonable simplifying approximation and has been used for optical preamplifier receivers by Marcuse [44,45], and also for spectrum-sliced systems using PIN receivers by Pendock and Sampson [53]. Moreover we also neglect any mismatches in the center wavelength of the filters/demultiplexers, and assume that both the transmitter and receiver filter have identical characteristics for a given value of the filter order. Also, we neglect intersymbol interference effects resulting from dispersion and/or electrical filtering in the transmitter and receiver.

## 5.1 Tunable Optical Fiber Filters

Tunable filters play a crucial role in contemporary and next-generation WDM systems; such filters provide a low-cost technique to demultiplex the wavelength-encoded channels at the receiver, and also aid in other WDM functions. The main categories of filters that are used in commercial and experimental systems include fiber refractive-index grating-based filters, Fabry-Perot and multilayer dielectric thin-film resonant cavity filters and acousto-optic filters.

### *a) Refractive-index grating-based optical fiber filters*

An optical fiber grating refers to a periodic refractive-index modulation in the core of the optical fiber which effects wavelength-selective modal coupling. In other words, an in-fiber grating reflects/transmits a selected band of wavelengths, with the center wavelength of the transmitted/reflected band depending on the grating parameters such as the length, periodicity and fabrication method. Conventional in-fiber gratings, commonly referred to as fiber Bragg gratings (FBGs), were first demonstrated by Hill *et al.* [61] in 1978 by prolonged exposure of a germano-silicate optical fiber core to counter-propagating high intensity laser radiation at 488 nm. This resulted in the formation of a narrow-band reflection filter in the core of the optical fiber, with the reflection spectrum dependent on

the grating periodicity. This technique however limited grating formation to periodicities dictated by the writing or exposure wavelength. In 1989, Meltz *et al.* demonstrated the transverse holographic approach for Bragg grating formation, by which the reflection filter passband could be designed to be centered at any wavelength, depending upon the application [62]. Such grating operation is based upon the coupling of forward and backward propagating guided core modes in the optical fiber, and thus grating periodicities are limited to a few microns. Recently, long period refractive gratings (LPG) were proposed and demonstrated by a research group at AT&T [63]. The larger periodicity of the grating effects coupling between the fundamental mode and the forward propagating cladding modes resulting in a broad bandstop filter in the transmission spectrum of the fiber, as opposed to FBG which results in a narrow bandpass filter in the reflection spectrum of the fiber. A schematic of the grating structure and typical filter shapes for the LPG and FBG are shown in Fig. 5.1.

The major applications of optical fiber gratings that are of interest to WDM system designers include:

- FBG and LPG can be tailored to provide stable narrowband and broadband filters for demultiplexing WDM channels and in other add-drop and wavelength conversion applications.
- The periodicity of the FBG can be chirped (*i.e.* made a function of length); a chirped grating then reflects different wavelengths along different parts of its length. A controlled design of the chirping function can be used to provide dispersion compensation by forcing different wavelengths of a dispersed pulse to travel different distances, thereby equalizing the effect of dispersion.
- LPGs were recently shown to be extremely attractive for gain-flattening of the EDFA spectrum [11]. A gain-flattened EDFA offers a lower distortion to the densely packed WDM channels that it simultaneously amplifies. (Conventional EDFAs, depending on their gain profiles, provide selective gain to some of the channels thereby distorting the power spectrum of the WDM waveform.)
- Reflection and transmission in-fiber gratings are extremely attractive for removing the unwanted pump signals and ASE in fiber amplifiers.

The parameter of most interest to us in the spectrum-slicing context is the passband of the fiber grating filter. This passband is a function of the exact profile of the refractive-index modulation impressed in the core of the photosensitive fiber. **The various techniques used during the grating fabrication process, such as chirping and apodizing essentially dictate the refractive index profile, and by controlling these two techniques, fiber Bragg gratings with virtually any desired passband can be fabricated** [64].

*b) Acousto-optic tunable filters (AOTF)*

AOTFs are based on the wavelength-selective diffraction of an incident light beam on a material with a high photoelastic constant, which is excited with an appropriate transducer to generate acoustic waves [6]. The acoustic wave produces periodic local compressions and rarefactions which results in the formation of a grating that can diffract an incident light beam to an angle which depends on the angle of incidence, the light wavelength, and the acoustic wavelength. AOTFs are an attractive candidate for WDM applications since they permit independent wavelength switching, as needed for reconfigurable all-optical networks [65].

*c) Waveguide Grating Routers*

Although bulk-optic or all-fiber filters and devices are used in a number of WDM applications, the trend is increasingly towards the monolithic integration of such devices and components. A generic device towards this end is the arrayed waveguide (AWG) multiplexer, also known as a waveguide grating router (WGR) [28]. The device is fabricated on InP and consists of input-output arrays, two free-space regions, and a waveguide grating array between the two free space regions. Light from one of the input ports expands in the free space regions and couples to the different grating arms. By making the grating arms of different lengths, a fixed path length difference is maintained between them, thereby effecting a wavelength-dependent phase shift. This linear phase progression affects the propagation directions of the of the optical wave as it radiates into the second free space region towards the output ports. Waveguide grating routers have been successfully demonstrated

for a number of WDM enabling devices such as multiplexers, channel dropping filters/equalizers, and tunable lasers [29]. (The WGR was also discussed in Section 1.3.2 and Fig. 1.5.)

*d) Fabry-Perot and thin-film resonant cavity filters*

Fiber Fabry-Perot (FP) filters have been used extensively in WDM applications because of their simple construction and ready availability. As shown in Fig. 5.2, the basic device operation is based on multiple reflections which take place in a dielectric sandwiched between two other dielectric materials [6]. The three materials form a FP cavity and provide a transmission and reflection spectrum due to constructive/destructive interference between the multiple reflections, which can be tuned mechanically to the wavelength of interest. Since the constructive interference phenomena is dependent on periodic multiples of the cavity length, multiple transmission peaks (fringes) are observed, with the wavelength difference between two consecutive fringes denoted as the free spectral range (FSR).

The normalized transmission characteristic for a Fabry-Perot filter, also shown in Fig. 5.2, is given by the relation [6]

$$T(\lambda) = \frac{1}{1 + (2F/\lambda)^2 \sin^2(2d\pi/\lambda)} \quad (5.1)$$

where  $F$  refers to the *fineness* of the FP cavity and is related to the reflectivity of the materials that form the cavity, and  $d$  is the length of the FP cavity. An important figure of merit is the bandwidth of the various transmission notches, which physically defines the amount of isolation that the filter can provide for rejecting interference from adjacent unwanted channels in the WDM system. The bandwidth of the FP filter is given by the ratio of the FSR to the fineness of the cavity. Recently, low-loss, environmentally-stable (with respect to temperature and humidity), and nearly square bandpass-profile filters were demonstrated by Scobey *et al.* from OCA, using a novel high vacuum physical vapor deposition process termed MicroPlasma [66].

### 5.1.1 Use of the Butterworth Filter Approximation

The parameter of most interest to us from the discussion on a fiber Fabry-Perot (FFP) filter is its passband. Although FFPs are simple to fabricate, their passband modeling for system simulation purposes is often hampered by their multiple passband resonances, as described by Eq. (5.1).

**However in the limit of high reflectivity, a single resonant passband of the FFP filter may be assumed to be approximately Lorentzian in shape.** This can easily be seen from Eq. (5.1), where in the limit of high reflectivity ( $\sin \theta \sim \theta$ ), the 3-dB passband becomes to  $\Delta \omega = c/2dF$ , which gives

$$T(\omega) = \frac{1}{1 + (2\omega / \Delta \omega)^2}. \quad (5.2)$$

Eq. (5.2) is identical to a Lorentzian passband. This equivalence is graphed in Fig. 5.3a for a cavity finesse of 5, and a FWHM of 1 nm.

**We make use of the same approximation for our analysis and take a further step to model all optical filters used in the transmission link to be of the general Butterworth type. This has two benefits. First of all, the Lorentzian passband is equivalent to the first order Butterworth filter. Secondly and more importantly, it facilitates our analysis when we wish to study the effect of varying the filter response (by increasing the order of the filter) on receiver sensitivity.** Moreover, Ngo and Binh recently demonstrated the analysis and fabrication of optical Butterworth bandpass filters, through combination of low-pass and high-pass filters made through phase-modulation of fiber optic interferometers and ring resonators [67].

In general, the magnitude squared transfer function of a Butterworth filter may be expressed as

$$|H_o(f)|^2 = \frac{1}{1 + (f/f_o)^{2N}} = \frac{1}{1 + (2f/B_o)^{2N}} \quad (5.3)$$

where:

$f$  = difference of frequency from the operating optical frequency (in Hz),

$f_o$  = 3 dB baseband bandwidth of the filter (in Hz),

$B_o$  = 3 dB bandpass bandwidth of the optical filter (in Hz), and

$N$  = order of the Butterworth filter

The normalized frequency response of various order  $N$  Butterworth filters is plotted in Fig. 5.3b. It is noted that lower order filters have slower passband to stopband roll-offs and larger tails, as compared with higher order filters which have sharper cut-offs. Very large orders of the filter then approach the passband of a rectangular filter.

## 5.2 Mathematical Formulation

As described in Chapter 3, the signal, comprising the square-law detected and electrically (integrate-and-dump) filtered spectrum-sliced information signal and the ASE noise from the preamplifier may be expressed in units of power as

$$I = \frac{1}{2T} \int_0^T [x^2(t) + y^2(t) + \tilde{x}^2(t) + \tilde{y}^2(t)] dt \quad (5.4)$$

Here  $x(t)$ ,  $y(t)$ ,  $\tilde{x}(t)$ , and  $\tilde{y}(t)$  are independent, identically distributed (i.i.d) baseband Gaussian processes with (optical) bandwidth  $B_o/2$ , having zero-mean, and each having a variance  $\sigma^2$  equal to the optical power contributed by *each* of the two orthogonal polarizations. Also  $T$  is the inverse data rate, or the time period over which the electrical filter integrates or adds the power. Note that the four terms within the integral correspond to two orthogonal phases and two orthogonal polarizations. We neglect shot noise terms since they will be negligible compared to the inherent signal fluctuation noise, and will also be negligible compared to the ASE noise for the optical preamplifier receiver. Also, for the optical preamplifier receiver, in the on-state,  $x$ ,  $y$ ,  $\tilde{x}$ , and  $\tilde{y}$  are the components of the noise-like signal plus the corresponding components of the preamplifier ASE. In the off-state these are just the components of the preamplifier ASE noise. We assume that the preamplifier gain is sufficiently high that the electrical thermal noise may be neglected.

Now the objective of the following analysis will be to fit the first two moments of  $I$  to standard distributions (Gaussian, Chi-square) which will facilitate the calculation of the receiver sensitivity. Accordingly, the mean of  $I$  is given by

$$\langle I \rangle = \frac{1}{2T} \left( 4 \int_0^T dt \right) = 2 \int_0^T dt. \quad (5.5)$$

To evaluate the variance terms, we use the analysis originally developed by Jacobs [68] with slight modifications to account for the noise-like nature of the spectrum-sliced signal, and two polarizations instead of the one used in that work. The variance of  $I$  is given as

$$\text{var } I = \langle I^2 \rangle - \langle I \rangle^2. \quad (5.6)$$

The first term on the rhs of Eq. (5.26) may be evaluated for a single polarization first as

$$\langle I^2 \rangle = \frac{1}{2T} \int_0^T dt \int_0^T dt' \langle x^2(t) + y^2(t) + \tilde{x}^2(t) + \tilde{y}^2(t) \rangle \langle x^2(t') + y^2(t') + \tilde{x}^2(t') + \tilde{y}^2(t') \rangle \quad (5.7)$$

Because of the incoherent nature of the broadband source, we can use the following properties to evaluate the above equation:

$$i) \langle x \rangle = \langle y \rangle = 0, \quad (5.8)$$

$$ii) \langle x^2(t) \rangle = \langle y^2(t) \rangle = \frac{2}{N}, \quad \text{where the subscript } N \text{ refers to the order of the filter,}$$

$$iii) \langle x(t)x(t') \rangle = \langle y(t)y(t') \rangle = R(\tau), \text{ where } R(\tau) \text{ is the autocorrelation of the Gaussian process with the normalized autocorrelation being defined as } \hat{R}(\tau) = R(\tau)/R(0), \text{ and}$$

$$iv) \langle x^2(t)y^2(t') \rangle = \langle x^2(t')y^2(t') \rangle = \frac{4}{N}.$$

Hence using the above equations, the variance of  $I$  is

$$\text{var } I = \frac{1}{2T} \int_0^T dt \int_0^T dt' \left[ 4 \langle x^2(t)x^2(t') \rangle + 12 \frac{4}{N} T^2 - 4 \frac{4}{N} \right] \quad (5.9)$$

Note that the analysis applies to both 1 and 0 transmission and appropriate subscripts will be added later. To evaluate the first and second terms of Eq. (5.23), we employ the moment generating function, as applied to a bivariate Gaussian distribution [50]

$$M(\mu_1, \mu_2) = \exp \frac{1}{2} \left( \mu_1^2 + 2\hat{R}_{12} \mu_1 \mu_2 + \mu_2^2 \right) \quad (5.10)$$

with

$$\langle x^2(t)x^2(t') \rangle = \frac{4M}{2^2} \Big|_{\mu_1 = \mu_2 = 0} \quad (5.11)$$

Using Eq. (5.11) with Eqs. (5.10) and (5.8) [68]

$$\langle x^2(t)x^2(t') \rangle = 2 \frac{4}{N} \hat{R}^2(t-t') + \frac{4}{N} \quad (5.12)$$

which is used in Eq. (5.6) to get

$$\text{var } I = \frac{2}{T^2} \int_0^T \int_0^T dt dt' \frac{4}{N} \hat{R}^2(t-t') \quad (5.13)$$

Employing the transformation of coordinates, as shown in [68], and recognizing that  $\frac{2}{N} = R(0)$ , we finally obtain

$$\text{var } I = \frac{4}{T^2} \int_0^T d(T-t) R^2(t) \quad (5.14)$$

For spectrum-sliced systems the optical bandwidth is generally much larger than the bit rate which leads to a wide power spectrum, and hence a narrow autocorrelation. This allows us to

a) change the limits in Eq. (5.14) from  $[T,0]$  to  $[-\infty,0]$  and b) neglect  $\frac{1}{T}$  in comparison to  $T$ . Using this approximation

$$\text{var } I = \frac{2}{T} \int_{-\infty}^0 d R^2(t) \quad (5.15)$$

Finally use of Parseval's theorem allows us to express Eq. (5.15) in terms of the power spectrum of  $I$  as

$$\text{var } I = \frac{2}{T} \int_{-}^{\infty} df |P(f)|^2 . \quad (5.16)$$

Note that in the above equation,  $\text{var } I$  is the variance accounting for both polarizations whereas, because of the way the autocorrelation function is defined (Eq. 5.8),  $P(f)$  is the equivalent baseband power spectrum in a single polarization only.

In the following sub-sections we will investigate how the signal and noise paths can be expressed in terms of the filter parameters and employ the resultant power spectrum, as described in Eq. (5.16), to calculate the receiver sensitivity.

### 5.2.1 Signal Path in Terms of Filter Parameters

A schematic of the system under consideration is shown in Fig. 5.4. As illustrated in the figure, a broadband noise source, assumed to be white over the wavelength band of interest if spectrally-sliced by an optical filter at the transmitter. **The primary objective of system design here is to minimize the average number of transmitted spectrum-sliced photons per bit, i.e. the output of the transmitter optical filter.** Defining  $P_o$  as the single-sided, single-polarization, power spectral density of the source, scaled by the attenuation of the fiber, we can write the following equation:

$$P_o B_{o,eqv,N} = \overline{N}_p h R_b \quad (5.17)$$

where  $B_{o,eqv,N}$  represents an equivalent rectangular bandwidth of the transmitter optical filter which allows the same amount of power to pass as the Butterworth filter. The rhs of Eq. (5.17) is the average single-polarization power with  $h$  being the photon energy and  $R_b$  being the system bit rate. The equivalent bandwidth may be calculated by

$$B_{o,eqv,N} = \frac{1}{|H_o(0)|^2} \int_{-}^{\infty} |H_o(f)|^2 df . \quad (5.18)$$

This may be readily evaluated using the Butterworth transfer function defined in Eq. (5.3) to get

$$B_{o,eqv,N} = \frac{B_o}{2N \sin(\pi/2N)} = C_{eqv,N} B_o \quad (5.19)$$

with  $B_o$  being the 3 dB bandwidth of the Butterworth filter. Hence using Eqs. (5.19) and (5.17), the PSD of the source can be expressed as

$$P_o = \frac{\overline{N_p} h R_b}{C_{eqv,N} B_o} \quad (5.20)$$

The spectrum-sliced signal now passes through an ideal (dispersionless, linear in power) fiber link, and is then preamplified and passed through an ASE suppresser/WDM selector filter at the receiver. **The signal channel is then given by the cascade of the two optical filters.**

Assuming the filters are centered identically, the channel (transmitter and receiver optical filters) filters the transmitter PSD, and thus the optical power spectrum (in one polarization) at the photodetector may be expressed as

$$P_s(f) = P_o G |H_o(f)|^2 |H_o(f)|^2 \quad (5.21)$$

since the output PSD of a random process is the product of the input PSD and the *magnitude squared* of the transfer function of the channel. Also here the  $G$  term accounts for the power gain of the optical preamplifier. Using the above equation, the average signal power at the photodetector, due to the signal component alone and accounting for both of its polarizations, is given by

$$P_s = 2 \int_{-B_o}^{B_o} P_s(f) df. \quad (5.22)$$

Here  $\int_{-B_o}^{B_o} P_s(f) df$  is the signal power per polarization (during a 1 transmission) and the subscript  $N$  refers to the signal power being a function of the order  $N$  of the filter being employed. Solving Eq. (5.22) using the general Butterworth transfer function given in Eq. (5.3), we get

$$P_s = 4P_o G \int_{-B_o}^{B_o} \frac{1}{\left[1 + (2f/B_o)^{2N}\right]^2} df = 2P_o G C_{sN} B_o \quad (5.23)$$

where the factor  $C_{sN}$  shows the effect of the filter order on the signal power and is given by

$$C_{sN} = \frac{(2N-1)}{4N^2 \sin(\pi/2N)}. \quad (5.24)$$

Finally using the above equations

$$N_{sN}^2 = P_o G C_{sN} B_o. \quad (5.25)$$

### 5.2.2 Noise Path in Terms of Filter Parameters

As illustrated in Fig. 5.4, the ASE noise generated at the optical preamplifier persists for both the 1 and 0 bits, and its effect is mitigated with the use of the ASE suppressor/WDM selector filter. The single-sided, single polarization ASE noise PSD at the output of the preamplifier is expressed as

$$N_o = n_{sp} h (G-1) \quad (5.26)$$

where  $n_{sp}$  is the spontaneous emission factor and defines the noise performance of the preamplifier. The noise power spectrum appearing at the photodetector is then

$$P_n(f) = N_o |H_o(f)|^2 \quad (5.27)$$

with the total noise power including both polarizations being

$$P_n = 2 N_{nN}^2 = 2 \int P_n(f) df \quad (5.28)$$

where  $N_{nN}^2$  is the noise power in one polarization. **Recognizing that the noise passes through only one filter** with the passband given in Eq. (5.3), the noise power may be evaluated to be

$$P_n = 4N_o \int_0^{B_o} \frac{1}{[1 + (2f/B_o)^{2N}]^2} df = 2N_o C_{nN} B_o \quad (5.29)$$

where the factor  $C_{nN}$  shows the effect of the filter order  $N$  and is given by

$$C_{nN} = \frac{1}{2N \sin(\pi/2N)}. \quad (5.30)$$

Hence using the above equations

$$N_{nN}^2 = N_o C_{nN} B_o. \quad (5.31)$$

### 5.3 OOK Transmission Analysis

In this section we will focus on evaluating the effect of the channel non-ideal frequency response, as characterized by the Butterworth transmitter and receiver optical filters, on receiver sensitivity. This is performed here for the case of OOK transmission. Analysis using both the Gaussian approximation and assuming chi-square statistics is discussed.

#### 5.3.1 Gaussian Approximation

Use of the Gaussian approximation to calculate the error probability implies evaluating the mean and variances of the signal and noise at the decision circuit, and fitting these moments to a Gaussian distribution. The mean (average) power during the 1 (spectrum-sliced signal + ASE noise) and 0 bits (ASE noise only) is

$$\mu_1 = 2 \left( \frac{2}{sN} + \frac{2}{nN} \right) \quad \mu_0 = 2 \left( \frac{2}{nN} \right). \quad (5.32)$$

To calculate the system  $Q$ , it is necessary to evaluate the noise variance during the 1 and 0 bits.

This is done as follows.

*i) 0 bit transmission*

Using Eq. (5.16) for the variance and Eq. (5.27) for the power spectrum of the noise we have

$$\text{var } I_0 = \frac{2}{T} \int |P_n(f)|^2 df = \frac{4}{T} N_o^2 \int \frac{1}{[1 + (2f/B_o)^{2N}]^2} df. \quad (5.33)$$

This results in

$$\text{var } I_0 = \frac{2N_o^2 K_{nN} B_o}{T} = \frac{2m}{T^2} N_o^2 K_{nN} \quad (5.34)$$

where  $m = B_o T$  and the factor  $K_{nN}$  represents the effect of the filter order  $N$  and is given by

$$K_{nN} = \frac{(2N-1)}{4N^2 \sin(\pi/2N)}. \quad (5.35)$$

ii) 1 bit transmission

Transmission of the 1 bit includes contributions from both the spectrum-sliced signal and the preamp ASE noise. The power spectrum now seen at the detector is hence the summation of the signal and noise spectrum. The variance may then be expressed as

$$\begin{aligned} \text{var } I_1 &= \frac{2}{T} \int_0^B |P_s(f) + P_n(f)|^2 df \\ &= \frac{4}{T} \int_0^B P_o^2 \frac{1}{[1 + (2f/B_o)^{2N}]^4} df + N_o^2 \int_0^B \frac{1}{[1 + (2f/B_o)^{2N}]^2} df + 2P_o N_o \int_0^B \frac{1}{[1 + (2f/B_o)^{2N}]^3} df \end{aligned} \quad (5.36)$$

which may be expressed in a form similar to the 0 bit variance as

$$\text{var } I_1 = \frac{2m}{T^2} [P_o^2 K_{sN} + N_o^2 K_{nN} + 2P_o N_o K_{snN}] \quad (5.37)$$

The associated constants appearing in the above equation are

$$K_{sN} = \frac{(6N-1)(4N-1)(2N-1)}{96N^4 \sin^2(1/2N)} \quad (5.38)$$

and

$$K_{snN} = \frac{(4N-1)(2N-1)}{16N^3 \sin^2(1/2N)} \quad (5.39)$$

Now that the signal and noise mean and variance terms are known, we can evaluate the  $Q$  factor as

$$Q = \frac{\mu_1 - \mu_0}{\sqrt{\text{var } I_1} + \sqrt{\text{var } I_0}} \quad (5.40)$$

Using Eq. (5.32) along with Eqs. (5.33) and (5.36), we get

$$Q = \frac{2 \mu_{sN}}{\sqrt{\frac{2m}{T^2} [\sqrt{P_o^2 K_{sN} + N_o^2 K_{nN} + 2P_o N_o K_{snN}} + \sqrt{N_o^2 K_{nN}}]}} \quad (5.41)$$

which, employing Eqs. (5.25) and (5.31), can be expressed as

$$Q = \frac{\sqrt{2m}}{\sqrt{bx^2 + 2cx + a} + \sqrt{bx^2}}. \quad (5.42)$$

Here

$$a = \left( K_{sN} / C_{sN}^2 \right) \quad b = \left( K_{nN} / C_{nN}^2 \right) \quad c = \left( K_{snN} / C_{sN} C_{nN} \right), \quad (5.43)$$

and for  $G \gg 1$

$$x = \frac{\frac{2}{nN}}{\frac{2}{sN}} = \frac{n_{sp} h (G-1)}{\bar{N}_p h R_b G} \frac{C_{nN}}{C_{sN} / [C_{eqv,N} B_o]} = \frac{n_{sp} m C_{nN} C_{eqv,N}}{\bar{N}_p C_{sN}}. \quad (5.44)$$

Note again that the  $C$  and  $K$  factors represent the contribution of the order  $N$  of the Butterworth filter. For high orders ( $N > 10$ ), these factors approach unity, as shown in Fig. 5.5, and then the above analysis reduces to the analysis performed earlier for the rectangular filter case.

Using the above equation and solving for the average receiver sensitivity, we get

$$\bar{N}_p = \frac{n_{sp} m (2cQ + \sqrt{8bm}) C_{nN} C_{eqv,N}}{\frac{2m}{Q} - aQ C_{sN}}. \quad (5.45)$$

This is plotted in Fig. 5.6 for the error probability  $P_e = 10^{-9}$  ( $Q = 6$ ), and  $n_{sp} = 2$ , and at various values of  $N$ . The results indicate the receiver sensitivity degrades ( $\bar{N}_p$  becomes larger) as the order of the filter is reduced. The major reason for this result is that as the order of the filter is reduced, the noise power starts increasing relative to the signal power. This is because the noise passes through only one filter whereas the signal passes through two filters. As shown explicitly in Eq. (5.45),  $\bar{N}_p$  is proportional to the ratio  $(C_{nN} C_{eqv,N}) / C_{sN}$ . Fig. 5.5 shows that as  $N$  reduces,  $C_{nN}$  and  $C_{eqv,N}$  both increase, whereas  $C_{sN}$  reduces. The increase of  $C_{nN}$  refers to an increase in the noise power; increase in  $C_{eqv,N}$  reduces the signal PSD and hence reduces the signal power; and a reduction in  $C_{sN}$  means that signal power reduces. Hence the combined effect of this ratio, as plotted in Fig. 5.7, is to degrade the receiver sensitivity as the order  $N$  of the filter reduces.

Also, as seen in Chapter 3, the Gaussian approximation predicts error floors for  $m < aQ^2/2$ .

### 5.3.2 Chi-Square Analysis

As asserted throughout this dissertation, a more reasonable approximation of the spectrum-sliced signal at the decision circuit is based on chi-square rather than Gaussian statistics. The chi-square distribution is defined by the number of degrees of freedom ( $m$ ), and the variance ( $\sigma^2$ ) of the Gaussian process at the input to the square-law receiver. For the case of ideal or rectangular spectra, the  $m$  values for when a 1 and a 0 are transmitted are the same, and were represented as  $m$  in the previous chapters. This situation changes when the effect of practical filter shapes is being analyzed. In this case, the degrees of freedom are now weighted by the combined frequency response of the filters appearing between the source of the signal/noise and the photodetector. Note that in this chapter we will represent the 1 and 0 bit chi-square degrees of freedom as  $m_1$  and  $m_0$ , and reserve the use of  $m$  to represent  $B_o T$  with  $B_o$  being the 3 dB (bandpass) bandwidth of the transmitter and receiver optical filter. The objective, again, is to evaluate the average receiver sensitivity  $\bar{N}_p$  in terms of  $m$ .

To relate the degrees of freedom to the filter parameters, we note from Eq. (3.14) of Chapter 3 that the variance of  $I$  can be written in terms of the degrees of freedom as

$$\text{var } I_{(1/0)} = \frac{2 \binom{4}{(1/0)N}}{m_{(1/0)}}. \quad (5.46)$$

where the subscripts (1/0) represent the corresponding bit under consideration, and  $N$  reminds us of the effect of the order of the filter. Also

$$\binom{4}{1N} = \left( \binom{2}{sN} + \binom{2}{nN} \right)^2 \quad \binom{4}{0N} = \left( \binom{2}{nN} \right)^2. \quad (5.47)$$

which allows us to write, using Eq. (5.16) for the variance during 1 transmission:

$$m_1 = \frac{2 \left( \binom{2}{sN} + \binom{2}{nN} \right)^2}{\frac{2m}{T^2} \left( P_o^2 K_{sN} + N_o^2 K_{nN} + 2P_o N_o K_{snN} \right)}. \quad (5.48)$$

To simplify further analysis, we use the  $a$ ,  $b$ ,  $c$ , and  $x$  factors defined earlier in Eqs. (5.43) and (5.44) to write the number of degrees of freedom during the 1 bit transmission as

$$m_1 = \frac{m(1+x)^2}{bx^2 + 2cx + a} \quad (5.49)$$

Similarly for 0 transmission

$$m_0 = \frac{2 \left( \frac{2}{nN} \right)^2}{\frac{2m}{T^2} (N_o^2 K_{nN})} \quad (5.50)$$

which can be simplified to

$$m_0 = \frac{m}{b} \quad (5.51)$$

As a quick check note that for large orders of the optical filter, all factors  $a$ ,  $b$ , and  $c$  approach unity, and hence  $m_1 = m_0 = m$ .

For OOK when a 1 is transmitted, the photocurrent consists of signal + noise, both of which are individually chi-square distributed. HOWEVER, their sum is not strictly chi-square. This implies that our assumption of both 1 and 0 transmission being chi-square is merely a simplifying approximation and a more exact result will actually require us to compute the equivalent pdf of the convolution of two chi-square distributions. BUT we still believe that the analysis presented above, although not “exact” will be a better approximation than the Gaussian. Hence assuming that for both the 1 and 0 transmission will result in chi-square distributed processes at the decision circuit, the associated pdf is given by

$$P(x) = \frac{\left( \frac{m}{2} \right)^{2m}}{(2m)} x^{2m-1} \exp \left( -\frac{mx}{2} \right) \quad (5.52)$$

Now for OOK, the detection process is to fix a threshold and compare the received energy with that threshold. The optimum threshold is where the pdf's for the 1 and 0 transmission processes are equal. Making that choice gives the following transcendental equation for evaluating the pdf's.

$$\begin{aligned} x_{th} \left( \frac{m_o}{2} - \frac{m_1}{2} \right) + (2m_1 - 2m_o) \ln(x_{th}) \\ = 2m_o \ln \left( \frac{m_o}{2} \right) - 2m_1 \ln \left( \frac{m_1}{2} \right) + \ln \left( \frac{2m_1}{2m_o} \right) \end{aligned} \quad (5.53)$$

For large values of  $m$ , the gamma function (last term in rhs of the above equation) often blows up due to the limited capabilities of the numerical analysis software. To minimize the effect of this possibility, we used the following standard relationship for gamma functions [69]

$$\Gamma(2x) = \frac{2^{2x-1} \Gamma(x) \Gamma(x+0.5)}{\sqrt{\pi}} \quad (5.54)$$

which helped us to write

$$\ln \frac{\Gamma(2m_1)}{\Gamma(2m_o)} = (m_1 - m_o) \ln(4) + \ln \frac{\Gamma(m_1)}{\Gamma(m_o)} + \ln \frac{\Gamma(m_1 + 0.5)}{\Gamma(m_o + 0.5)}. \quad (5.55)$$

The methodology for deriving an expression for the error probability for an OOK spectrum-sliced system with an optical preamplifier was described earlier (see Section 3.5). We modify those results to take into account the case of non-rectangular spectra to get

$$P_e = \frac{1}{2} \left[ 1 - \frac{\Gamma(m_o)}{\Gamma(m_o + 1)} x_{th, 2m_o} + \frac{\Gamma(m_1)}{\Gamma(m_1 + 1)} x_{th, 2m_1} \right] \quad (5.56)$$

where  $\Gamma(x)$  is the incomplete gamma function. This is plotted in Fig. 5.8 for the error probability  $P_e = 10^{-9}$  and  $n_{sp} = 2$ , and for  $N = 1, 2, 3, 4, 5$ , and 100 (rectangular spectra case). The results are similar to those obtained using the Gaussian approximation, *i.e.* show that receiver sensitivity degrades when the order of the filter is reduced. The major reason for this trend was discussed at the end of Section 5.3. In terms of the absolute magnitude of receiver sensitivity, the chi-square predicts lower values of  $\bar{N}_p$  than does the Gaussian, and does not display any error floors unlike the Gaussian - both observations are consistent with the results in Chapter 3.

Another interesting observation from Fig. 5.8 is that although the  $N = 1$  case (361 ph/b) requires a higher value of  $\bar{N}_p$  as compared with the rectangular spectra case (230 ph/b), the

required value of  $m$  is *lower* ( $m = 26$  for  $N = 1$  and  $m = 33$  for  $N = 100$ )<sup>1</sup>. Although this result implies that a lower order of filter will need a lower bandwidth and will result in a larger transmission capacity for a given source bandwidth, one also has to recognize that lower order Butterworth filters have larger tails and may introduce a larger amount of interchannel interference. Hence a complete system analysis will have to take into account both the smaller value of optical bandwidth, and the larger value of interchannel interference, when the  $N = 1$  filter is considered for implementation in a spectrum-sliced system.

## 5.4 FSK Transmission Analysis

In this section we discuss the receiver sensitivity of spectrum-sliced FSK systems using optical preamplifier receivers and non-rectangular transmitter and receiver optical filters. The methodology used is similar to that for analyzing OOK transmission.

### 5.4.1 Gaussian Approximation

The Gaussian approximation involves knowledge of the mean ( $\mu_{(1/0)}$ ) and the variance during the 1 and 0 transmission. Following the procedure outlined in Section 2.4.3, we may write the following:

$$\mu_1 = -\mu_0 = 2 \frac{2}{sN} \quad (5.57)$$

and

$$\text{var } I_1 = \text{var } I_0 = \frac{2}{T} \int |P_s(f) + P_n(f)|^2 df + \int |P_n(f)|^2 df \quad (5.58)$$

where the first integral represents the variance in the channel containing the signal and the preamplifier ASE noise, whereas the second integral corresponds to the other channel which has ASE noise only. Using the  $C$  and  $K$  factors described in Section 5.3, we can simplify the above in the form

---

<sup>1</sup> Note that this difference only exists when the  $N = 1$  and the rectangular case are compared, and that higher orders of the filter require about the same value of  $m$  as the rectangular filter case. The difference is still of interest because the  $N = 1$  case corresponds to the Fabry-Perot filter which is commonly used in optical transmission systems.

$$\text{var } I = \frac{2}{m} \left[ \frac{4}{sN} \frac{K_{sN}}{C_s^2} + 2 \frac{4}{nN} \frac{K_{nN}}{C_n^2} + 2 \frac{2}{sN} \frac{2}{nN} \frac{K_{snN}}{C_s C_n} \right]. \quad (5.59)$$

Hence the  $Q$  factor may be written as

$$Q = \frac{\sqrt{2m}}{\sqrt{2bx^2 + 2cx + a}} \quad (5.60)$$

with

$$a = \left( K_{sN} / C_{sN}^2 \right) \quad b = \left( K_{nN} / C_{nN}^2 \right) \quad c = \left( K_{snN} / C_{sN} C_{nN} \right), \quad (5.61)$$

and

$$x = \frac{\frac{2}{nN}}{\frac{2}{sN}} = \frac{n_{sp} h (G-1)}{(\bar{N}_p/2) h R_b G} \frac{C_{nN}}{C_{sN} / [C_{eqv,N} B_o]} = \frac{2n_{sp} m}{\bar{N}_p} \frac{C_{nN} C_{eqv,N}}{C_{sN}}. \quad (5.62)$$

The average sensitivity  $\bar{N}_p$  is divided by a factor of two since, for FSK, the peak and average receiver sensitivity are the same, which means that the signal power per polarization ( $\frac{2}{sN}$ ) is *half* of the peak or average power. Thus solving for  $\bar{N}_p$  gives

$$\bar{N}_p = \frac{4n_{sp} m Q}{\sqrt{4mb + (c^2 - 2ab)Q^2} - cQ} \frac{C_{nN} C_{eqv,N}}{C_{sN}}. \quad (5.63)$$

This is plotted in Fig. 5.9 for the error probability  $P_e = 10^{-9}$  ( $Q = 6$ ), and  $n_{sp} = 2$ , and at various values of  $N$ . Similar to OOK, the results indicate the receiver sensitivity degrades ( $\bar{N}_p$  becomes larger) as the order of the filter is reduced. Also error floors are predicted at  $m < aQ^2/2$  which is exactly the same as predicted by the OOK analysis.

#### 5.4.2 Chi-Square Analysis

For FSK, since both the 1 and 0 imply signal + noise at the receiver, the corresponding effective degrees of freedom are the same and may be expressed as (using the nomenclature introduced in Section 5.3)

$$m_1 = m_0 = m_F = \frac{2^4}{\text{var } I} = \frac{m \left( \frac{2}{sN} + \frac{2}{nN} \right)^2}{\left[ a \frac{4}{sN} + 2b \frac{4}{nN} + 2c \frac{2}{sN} \frac{2}{nN} \right]} \quad (5.64)$$

which simplifies to

$$m_F = \frac{m(1+x)^2}{[2bx^2 + 2cx + a]} \quad (5.65)$$

Hence assuming that both the 1 and 0 transmission result in chi-square distributed samples at the decision circuit, and using the procedure outlined in Chapter 4, the probability of error for FSK transmission is

$$P_e = \frac{(m_F)^{4m_F}}{[(2m_F)]^2} \int_0^x \frac{1}{\frac{4m_F}{1N}} y^{2m_F-1} \exp\left(-m_F y / \frac{2}{1N}\right) dy - \frac{1}{\frac{4m_F}{0N}} x^{2m_F-1} \exp\left(-m_F x / \frac{2}{0N}\right) dx \quad (5.66)$$

where, for FSK, assuming that the “signal” is in channel 1

$$\frac{2}{1N} = \frac{2}{sN} + \frac{2}{nN} \quad (5.67)$$

and

$$\frac{2}{0N} = \frac{2}{nN} \quad (5.68)$$

Finally, using the approximation procedure described in Appendix B, the error probability may be written in a simplified way as (for  $m > 5$ )

$$P_e \approx \frac{1}{\sqrt{8 m_F}} \frac{4^{2m_F}}{(1+x)^{4m_F-1}} \quad (5.69)$$

where

$$= \frac{\frac{2}{0N}}{\frac{2}{1N}} = \frac{\frac{2}{nN}}{\frac{2}{sN} + \frac{2}{nN}} = \frac{x}{1+x} \quad (5.70)$$

with  $x$  defined in Eq. (5.62). Hence the combination of the two equations written above allow the evaluation of the average receiver sensitivity  $\bar{N}_p$ , as a function of  $m$ , at various error probabilities, and for any  $N$ . This is plotted in Fig. 5.10 for the error probability  $P_e = 10^{-9}$  and  $n_{sp} = 2$ , and at various values of  $N = 1, 2, 3, 4, 5$ , and 100 (corresponding to the rectangular spectra case). The

results show a trend similar to OOK - the receiver sensitivity degrades monotonically as the order of the filter is reduced.

#### 5.4 OOK vs. FSK

The analysis outlined above allows us to draw some simple comparisons between spectrum-sliced OOK and FSK transmission, when practical filter shapes are taken into consideration. First of all we compare the optimum values of  $m$  for which the receiver sensitivity reaches its minimum value. Fig. 5.11 illustrates the optimum  $m$  as a function of the filter order  $N$ . Similar to the observations of Section 4.4 of the previous chapter, FSK needs a smaller value of  $m$ , for each filter, than does OOK. However, each FSK WDM channel requires two filters, and as per the prior results, is not as bandwidth efficient. Also, the optimum  $m$  does not change very much with a change in the order of the filter for FSK, but does *increase* with an increase in  $N$  for OOK.

Fig. 5.12 graphs the average receiver sensitivity at the optimum for FSK and OOK as a function of the filter order. Also shown is the peak receiver sensitivity for OOK. As we have pointed out previously, OOK will perform poorer on the basis of peak receiver sensitivity. Note that both the Gaussian and the chi-square approximations predict that the order of the filter has a stronger (degrading) effect on the receiver sensitivity of FSK (Figs. 5.9 and 5.10) as compared to OOK (Figs. 5.6 and 5.8). **One possible reason for this might be that the degrading effect of signal fluctuations, with their fewer number of degrees of freedom compared to the noise, persists for both the 1 and 0 bits for FSK, but only occurs during the 1 bit for OOK.**

Expressed in slightly different words, the decision statistic for FSK, formed by differencing the outputs of the two channels, has a distribution with means (during a 1 and a 0) which are the negatives of each other. The corresponding variances, on the other hand, are the same. As the order of the filter increases, the magnitudes of the means increases (filters allow more power), and the variance decreases (more spectrum allows more averaging of the signal/noise terms). BUT it is the increases in the means that dominates, and performance improves with an increase in  $N$ . On the other hand, for OOK, the test statistic has different means and different variances during the 1 and 0

transmission. Here, as the filter order increases, the mean and variances no longer change the same way as they do in FSK, and hence the corresponding receiver sensitivity is not as poor.

Another comparison of interest is the penalty when one considers practical as opposed to ideal, rectangular, filter shapes. Defining this penalty to be the ratio of the corresponding receiver sensitivities for a practical (small  $N$ ) and an ideal (or very large  $N$ ) case, we plot the dB penalties in Fig. 5.13. **The important points to note here are that the shape of the filter strongly determines the performance of the spectrum-sliced system - passage through two optical filters reduces the degrees of freedom of the “signal” relative to the degrees of freedom of the noise which only passes through one filter. However, overall system penalties may be kept to < 1 dB by employing  $N > 2$  order Butterworth-response optical filters.** These are the primary conclusions of this chapter.

## 5.5 Summary

In this chapter we analyzed the transmission performance of spectrum-sliced transmission systems when non-ideal optical filters are employed at the transmitter and receiver. It was shown that receiver sensitivity is highly dependent on the 3 dB bandwidths of the filters, but that system power penalties could be minimized by employing high orders (flatter in passband) of the optical filters. The above analysis is, to the best of our knowledge, the first such numerical evaluation of the effect of practical filter shapes on the transmission performance of spectrum-sliced systems employing optical preamplifier receivers.

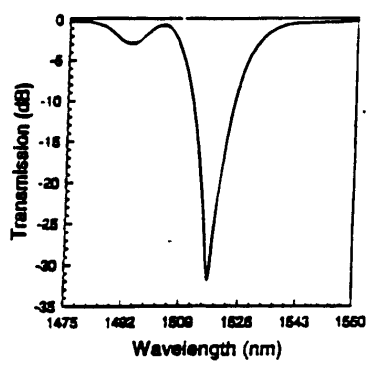
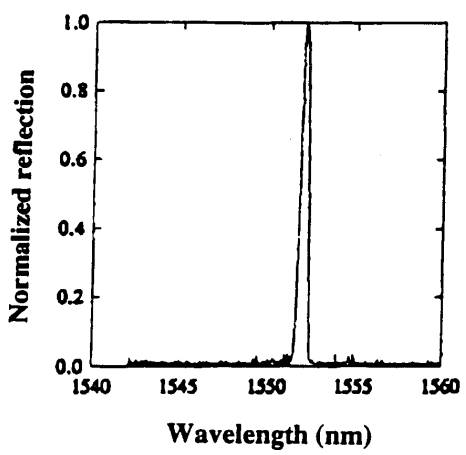
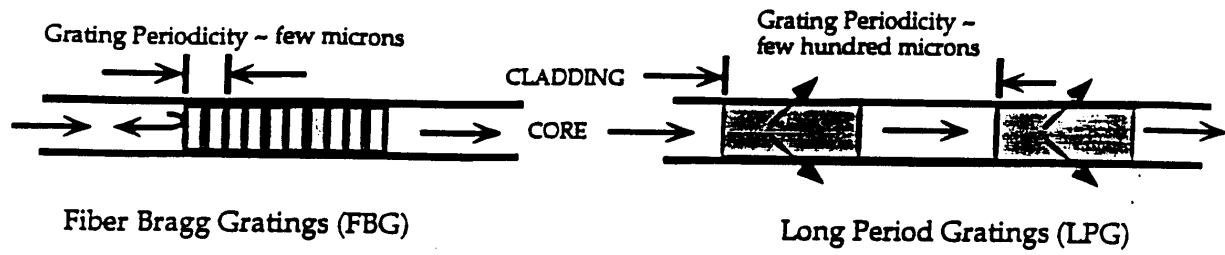


**Fig. 5.1:** Mode coupling and typical transmission (reflection) spectra for optical fiber Bragg and long-period grating filters.

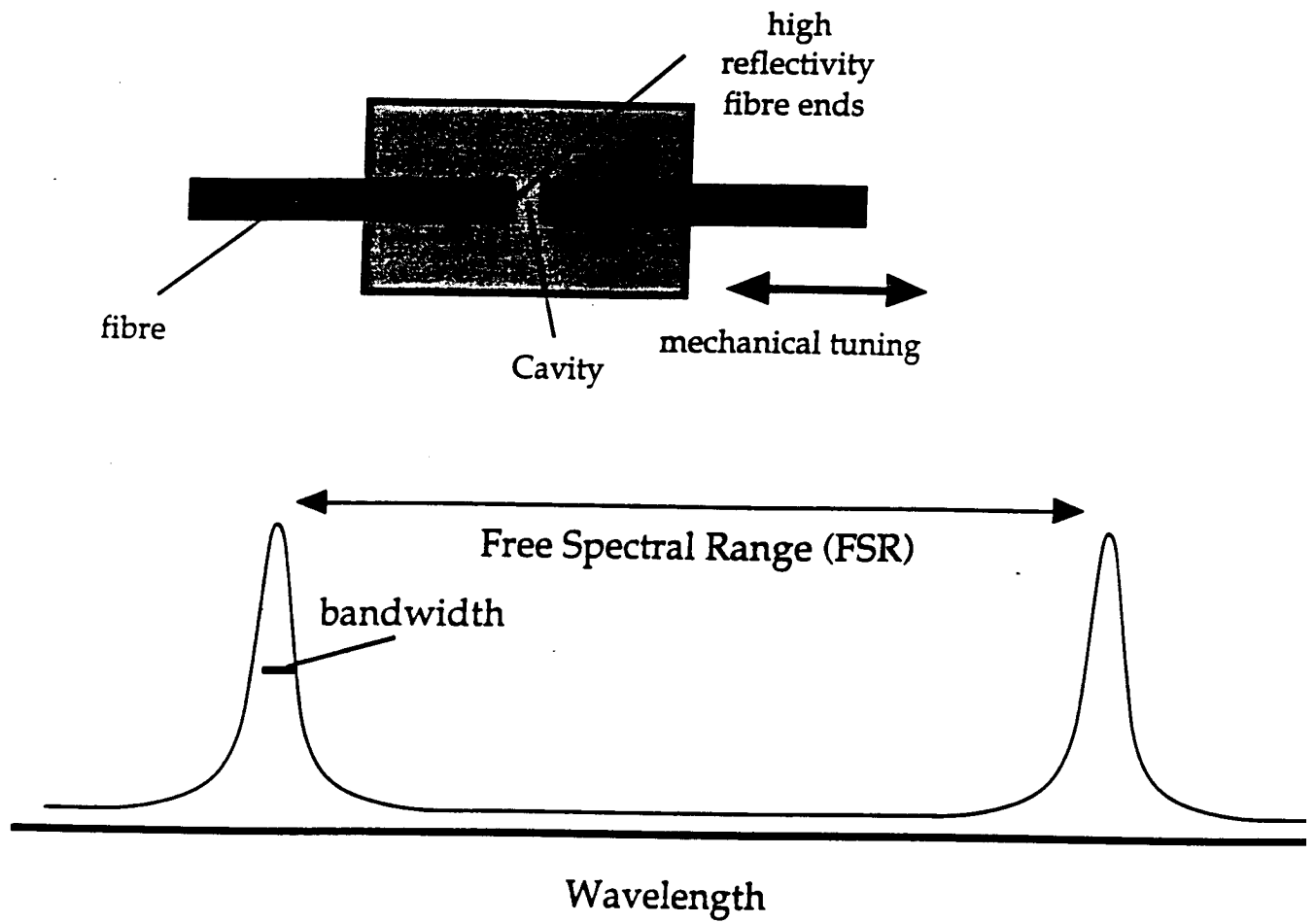


**Fig. 5.2:** *Fiber Fabry-Perot filter.*

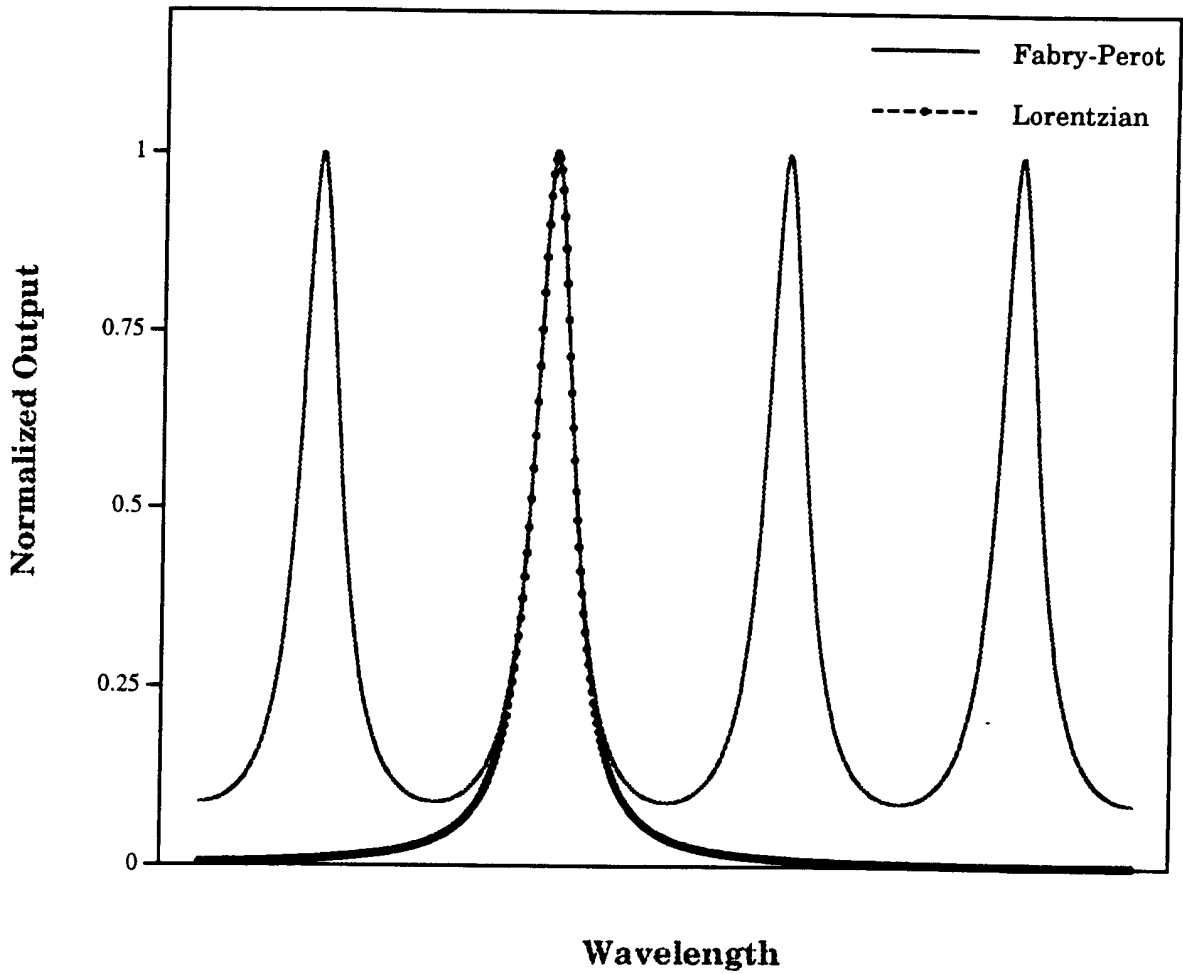


**Fig. 5.3a:** *Approximating a passband of a fiber Fabry-Perot filter with a Lorentzian lineshape (Finesse = 5, FWHM = 1 nm).*

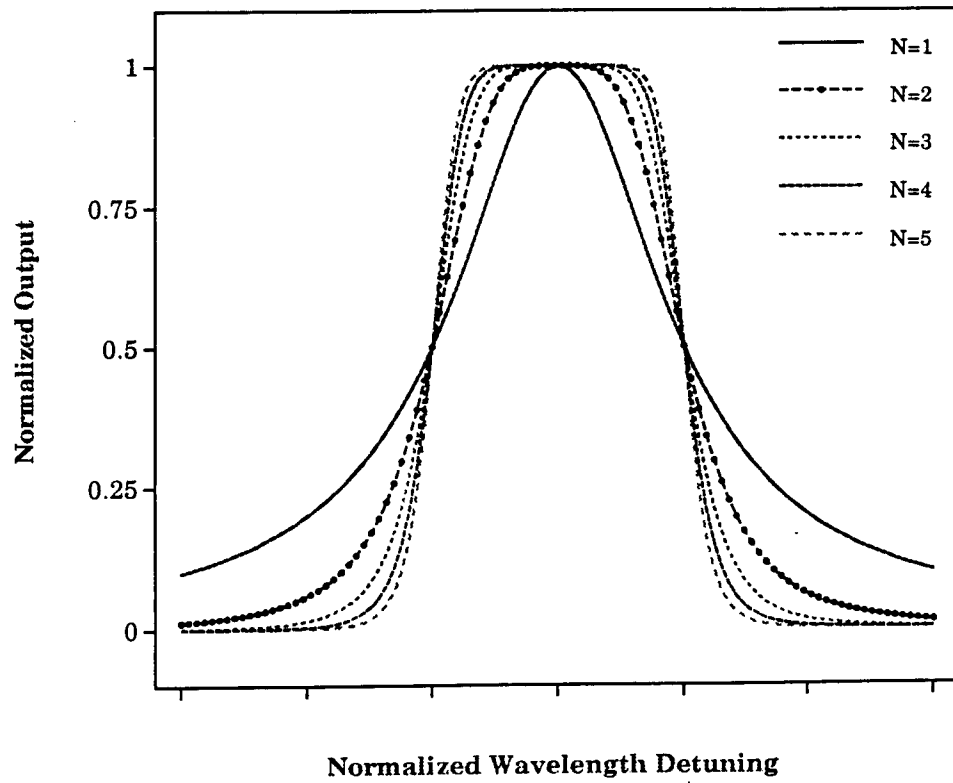


**Fig. 5.3b:** Normalized frequency response of various order  $N$  Butterworth filters.

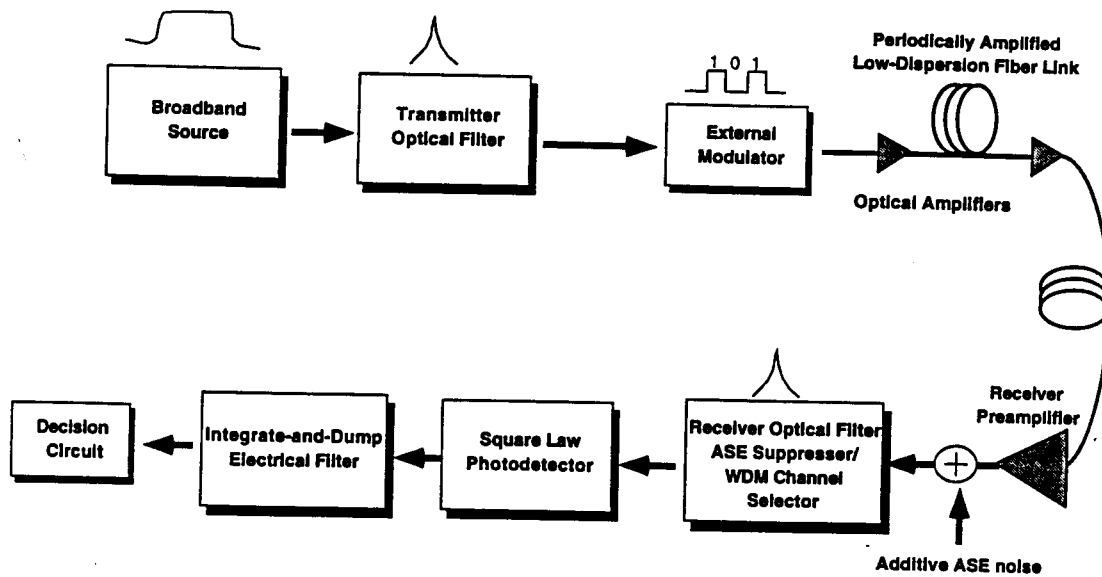


**Fig. 5.4:** Schematic of a spectrum-sliced system to illustrate the difference between the signal and noise paths.

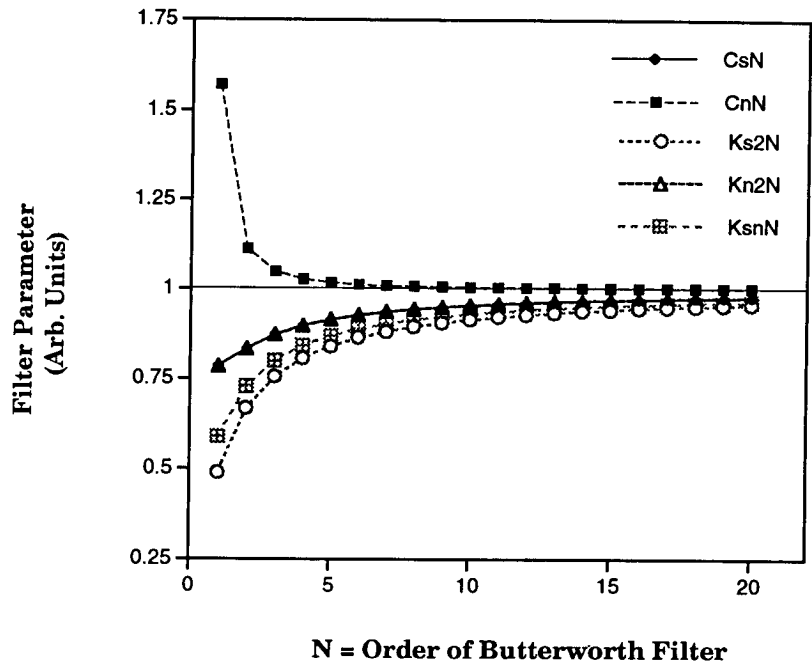


**Fig. 5.5:** Filter parameters as a function of the filter order  $N$ . Both signal and noise degrees of freedom become identical for very large orders of the filter, corresponding to the ideal (rectangular spectra) case.

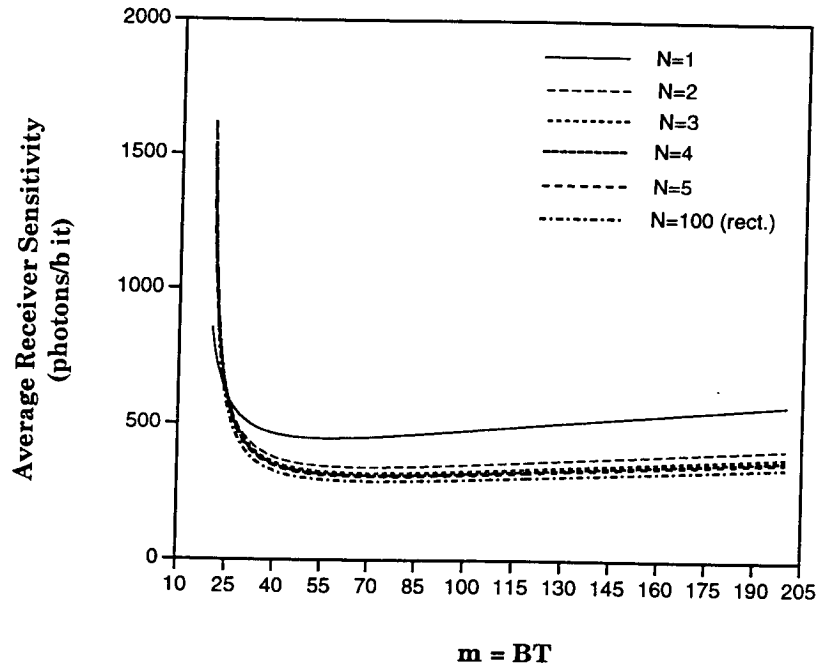


**Fig. 5.6:** Receiver sensitivity for an OOK transmission system using Butterworth filters of different orders  $N$ . Results are plotted using the Gaussian approximation.

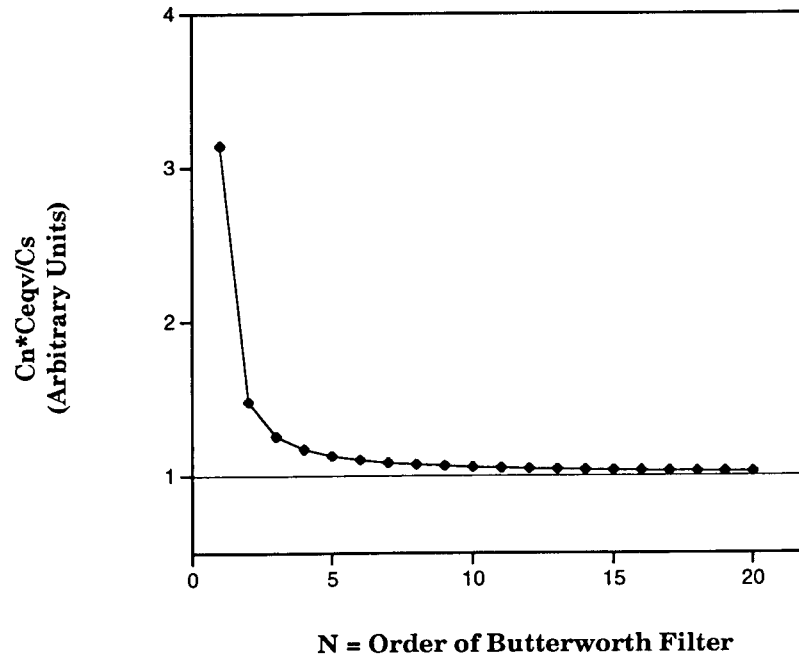


**Fig. 5.7:** Ratio of the noise to signal power as a function of the order of the filter.

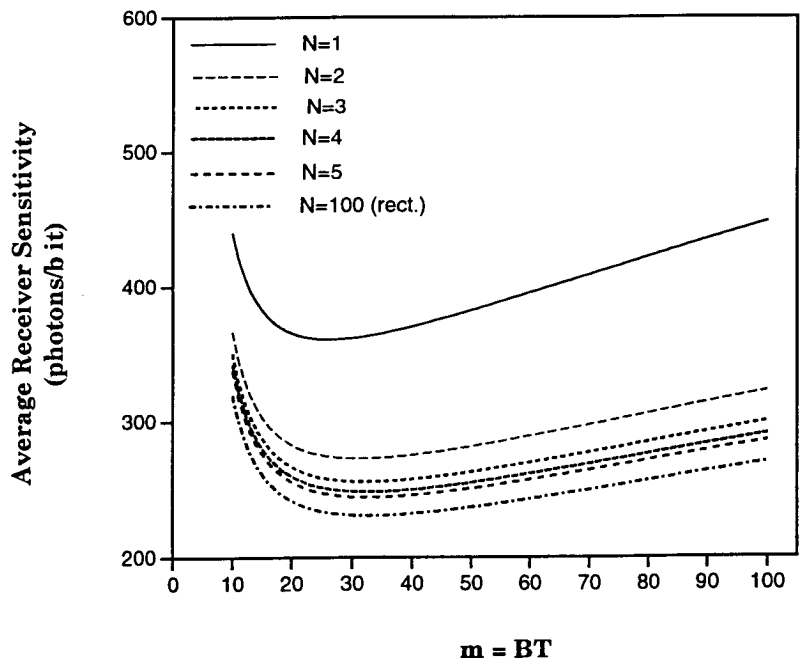


**Fig. 5.8:** Receiver sensitivity for OOK transmission at various orders  $N$  of the Butterworth filter, using the chi-square analysis.

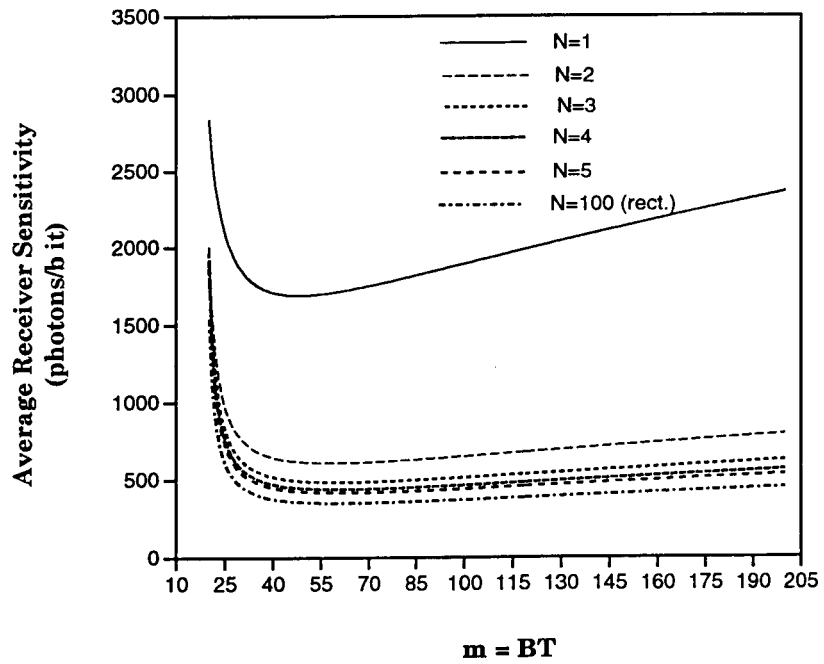


**Fig. 5.9:** Receiver sensitivity for spectrum-sliced FSK transmission system and optical preamplifier receiver detection, using the Gaussian approximation, and for various orders of the optical filters in the transmission path.

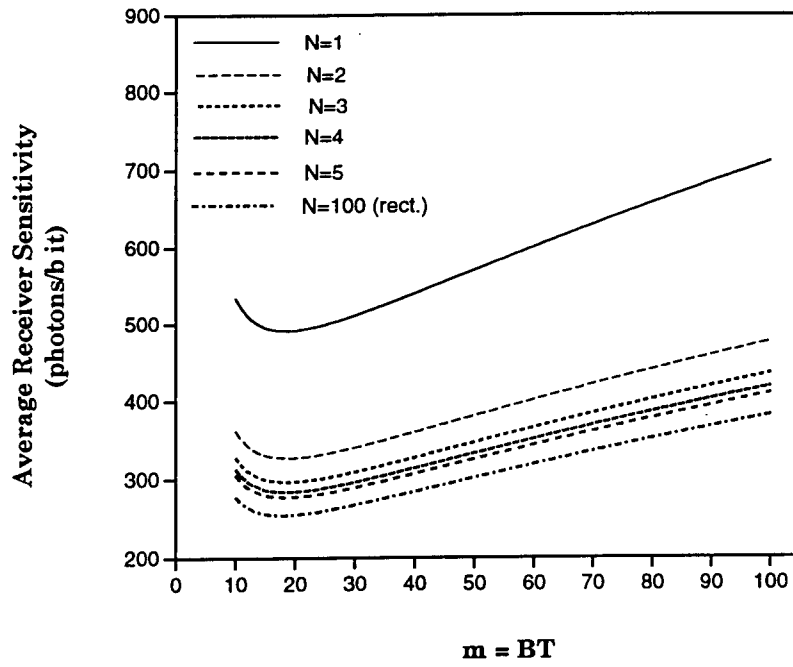


**Fig. 5.10:** Receiver sensitivity for FSK transmission at various orders  $N$  of the Butterworth filter, using the chi-square analysis.

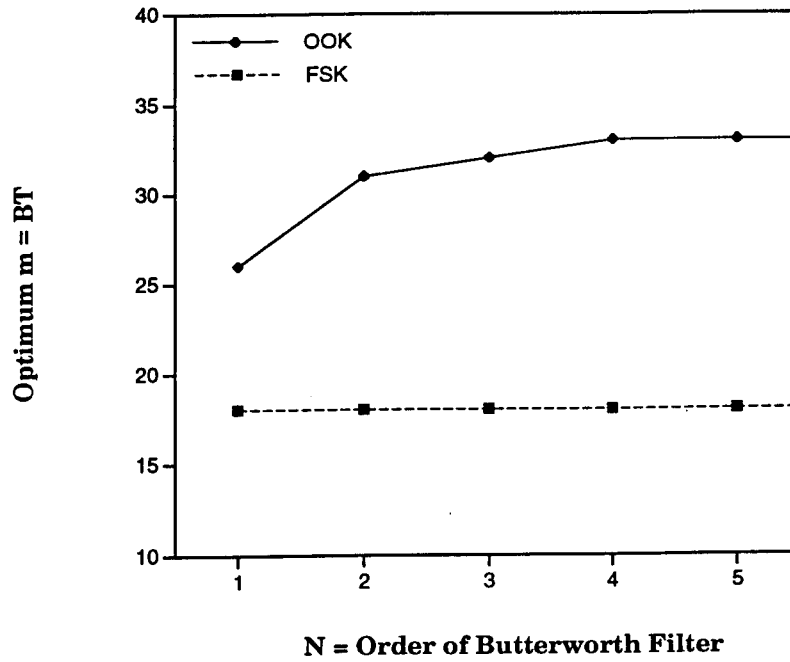


**Fig. 5.11:** Optimum  $m$  as a function of various filter orders for OOK and FSK, using the chi-square analysis.

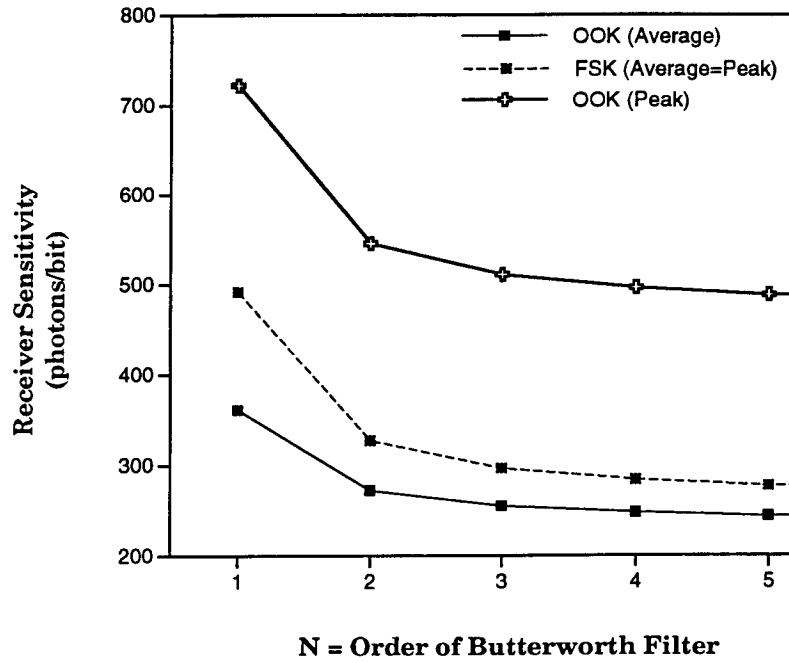


**Fig. 5.12:** Receiver sensitivity for OOK and FSK, also shown is the peak receiver sensitivity for OOK.

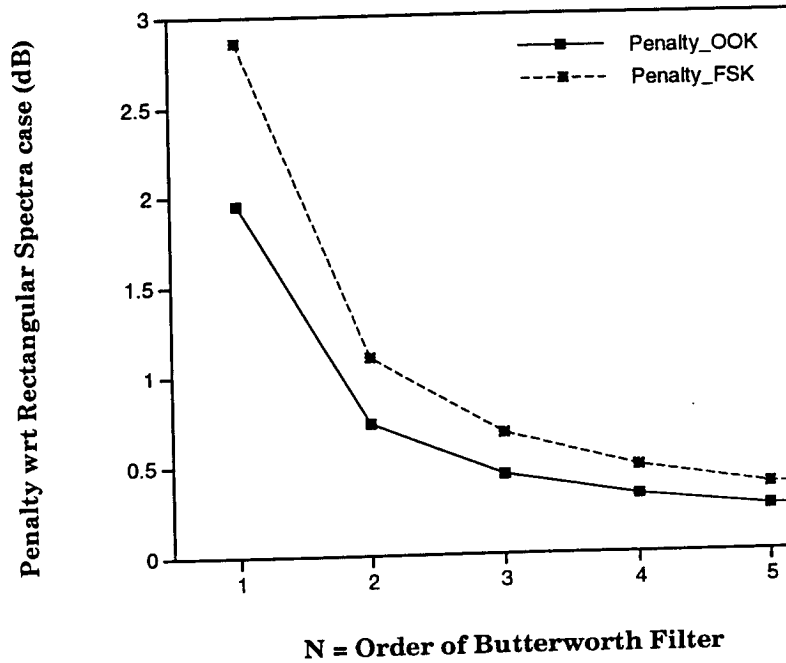


**Fig. 5.13:** Penalty with respect to the ideal (rectangular spectra) case; penalty reduces to less than 1 dB for  $N > 2$ .